NASA TECHNICAL MEMORANDUM

NASA TM X-68038

NASA TM X-68038

MOMENTUM FLUX IN TWO PHASE TWO COMPONENT LOW QUALITY FLOW

by Kenneth J. Baumeister, Robert W. Graham
Lewis Research Center
Cleveland, Ohio

and

Robert E. Henry
Argonne National Laboratory
Argonne, Illinois

TECHNICAL PAPER proposed for presentation at
Thirteenth National Heat Transfer Conference sponsored
by the American Institute of Chemical Engineers and the
American Society of Mechanical Engineers
Denver, Colorado, August 6-11, 1972

MOMENTUM FLUX IN TWO PHASE TWO COMPONENT LOW QUALITY FLOW

by Kenneth J. Baumeister, Robert W. Graham

Lewis Research Center
National Aeronautics and Space Administration
Cleveland, Ohio

and Robert E. Henry

Argonne National Laboratory
Argonne, Illinois

E-6871

ABSTRACT

In two phase flow systems line losses comprise frictional and momentum pressure drops. For design purposes, it would be desirable to estimate the line losses employing a one-dimensional calculation. In this paper two methods for computing one-dimensional momentum flux at a test section discharge station are compared to the experimental value for a range of two-phase flow conditions. The one-dimensional homogeneous model appears to be more accurate generally in predicting the momentum than the variable slip model.

INTRODUCTION

The pressure drop in a two phase flow system comprises frictional and momentum pressure drop. For a two phase system in which the fluid is being heated, the latter can be the most significant because of rapidly changing momentum accompanying void fraction increases. In this paper we are going to examine the validity of predicting momentum pressure drop by the use of a simple one-dimensional calculation.

Many analytical and experimental investigations have been devoted to studying two-phase pressure drop in a one-dimensional system. The most widely used analyses are those presented in references 1 and 2.

The possibilities of so many types of flow patterns in which the gaseous and liquid phases flow at different relative velocities has made it impossible to separate the momentum and frictional pressure drops to one universal theory. Consequently, there have been a variety of analytical models suggested which have been evaluated for specific two phase flow regimes. The simplest of the flow models has been the homogeneous, in which it is assumed that both phases are uniformly distributed across the diameter of the passage and both flow at the same velocity (no slip). The homogeneous model is usually treated as the reference one because of the relative ease with which it can be applied analytically. The more complicated models delineate possible variations in the void distribution and in the relative velocity between the phases (variable slip). While the more complicated models can relate more realistically to actual flows, there is always the question of how closely the simple homogeneous model will approximate certain properties of the flow - mainly pressure drop. Such an appraisal awaits more experimental information than has been generated thus far in which void, momentum pressure drop, total pressure drop, and flow rates are measured independently.

In reference 3, the authors measured the momentum flux discharge from a two component or a two phase flow in a pipe. For the two component case, they metered the air and water discharges; for the one-component case, they used a heat balance to estimate the liquid and vapor flow rates. The average void fraction was determined by isolating a section of transparent pipe by means of quick closing valves. One of the principle conclusions of reference 3 was that the one-dimensional modeling using measured void fractions (and variable slip) underpredicted

the system momentum and the homogeneous model, independent of the measured void and with no slip, yields a better estimate of momentum. The results did raise questions about the homogeneous model applicability to the data at the low quality regime. The authors raised the possibility of flow oscillations contributing to the disagreement between data and calculation.

High velocity data pressure drop reported in reference 4 and discussed in reference 5 indicate that one-dimensional modeling is quite acceptable at high system velocities. A composite of the experimental results of references 3 and 4 shows a definite velocity (Reynolds number) effect on the one-dimensional applicability. This effect is over and above that which is experienced in single phase flow as the flow transitions from a parabolic laminar velocity profile to a power law turbulent profile. This particular velocity dependence is a reflection of the system flow patterns and transitions (bubbly, slug, annular, mist, etc.).

Herein, one of the principle objects will be to perform a similar comparison between experimental data with the one-dimensional no slip (homogeneous) and variable slip representations for a range of velocities and void fractions.

Void fraction, flow rates of the gas and liquid species, and momentum discharge from the exit of the test section will all be measured independently. The void fraction measurement is made at a station just upstream of the test section discharge using the standard "one-shot" gamma attenuation technique. "One shot" means that the gamma beam is fixed at one position for all the tests.

The experimental momentum pressure drop results will be compared to the variable slip and the homogeneous model computations. The ranges of conditions wherein these models are suitable and wherein they are inaccurate will be discussed. The principle experimental information contained herein relates to the discharge momentum and the average void measured at the test section exit.

APPARATUS

The apparatus is diagramed in figure 1. The principal components comprise a test section, a nitrogen supply, and a water supply. The test section is a reinforced flattened tube with a gas-water mixer on one end for generating the two component flow. Flattening the test section confined the flow to an approximate one-dimensional pattern and increased the dimension in the direction of the gamma radiation, so as to increase the sensitivity of that measurement. The discharge from the open end of the test section was caught in a momentum cage enabling a measurement of the average force related to the momentum of the fluid discharge. A calibrated load or thrust cell was used to record the force. Figure 2 shows the construction of the momentum cage. It is an assembly of aluminum plates arranged to turn the flow discharged from the test section through an angle of 90^{o}. The cage is free-hanging, but is linked to the load cell behind it.

As is shown in figure 1, just upstream of the discharge point gamma radiation attenuation was used to measure the "one shot" void fraction. The gamma radiation was detected with a photomultiplier tube; the output was recorded on a strip-type recorder. A simple procedure in which a range of void blockages (lucite inserts with nearly the same attenuation

as water) were introduced into the gamma beam allowed the output of the photomultiplier tube to be checked. A linear reproducible curve shown in figure 3 resulted. The abscissa of figure 3, which is the void fraction determined from gamma attenuation, was determined from the simple expression

$$\alpha_{meas} = \frac{\ln \phi/\phi_f}{\ln \phi_o/\phi_f} \tag{1}$$

where ϕ_o, ϕ_f, and ϕ are the empty, full, and two-phase signals received from the photomultiplier sensor, respectively. Equation (1) was derived by Hooker and Popper (ref. 6). The derivation of equation (1) is based on the premise that the attenuation of a gamma beam is an exponential function of the absorption thickness. Henry (ref. 4) describes briefly other assumption inherent in equation (1) and estimates the errors associated with the use of this equation. Figure 3 shows good agreement between equation (1) and calibrated plastic voids which were introduced into the test section. During each run the all liquid and all gas conditions were compared. The signal strength ratios were consistently 1.29 which assured the operators that the void measuring system was on calibration.

Before the water and the nitrogen were introduced into the mixer, their flow rates and temperatures were monitored separately. Chromel-alumel thermocouples were used for the gas and water temperature measurements. The orifice flowmeters which were used for the flow measurement were calibrated in a standards laboratory. The pressure drop across the orifices was sensed by strain-gage type pressure transducers. It is estimated that the flow rates were known to within ±2 percent.

In a two phase flow system there is always the question of relative stability of the flow. Strip chart records of all the flow transducer measurements were made, and the mean values were used to compute the flow rate. In all of the runs there was some slow oscillation. This observation will be commented upon in discussing the results.

PROCEDURE

The experimental run conditions were established, generally, by deciding on a void fraction and then varying the gas and liquid rates to give that void fraction over a broad range of total flow rates. In actual practice the data points were set by watching the indication on the momentum measurement and then adjusting the gas and liquid flows so that the void measurement remained constant. From this procedure, a constant void curve was generated. This led eventually to a family of constant void curves covering a broad flow rate range.

All of the data were recorded on strip charts. Average values for each measurement were estimated and these values were utilized in the computerized calculation of the data.

CALCULATIONAL PROCEDURE

One-Dimensional Model (Measured α)

The momentum of the two phase, two component flow discharging from the test section was computed using a one-dimensional, two-phase equation (ref. 1 or 2). The equation for the discharge force (rate change of momentum) is

$$\overline{F}_{CAL} = \frac{W_w^2}{g_c \rho_w A(1 - \alpha)} + \frac{W_N^2}{g_c \rho_N A \alpha} \qquad (2)$$

where α is an experimentally determined value in this case. The force

produced by the nitrogen contribution in equation (2) was negligible compared to the water contribution. Consequently,

$$\overline{F}_{CAL} = \frac{W_w^2}{g_c \rho_w A(1 - \alpha)} \tag{3}$$

or in terms of the liquid Reynolds number

$$\overline{F}_{CAL} \approx \frac{R_w^2 P^2 \mu_L^2}{16 g_c \rho_w A(1 - \alpha)} \tag{4}$$

The results from this calculation were compared with the experimentally measured impulse obtained from the momentum cage-load cell arrangement at the discharge end of the test section.

Slip Ratio

The ratio of the average vapor to liquid velocity in a two phase system is commonly called the slip ratio, k. This ratio is related to the quality and void fraction by the expression

$$k = \frac{\rho_L}{\rho_v} \frac{x}{1 - x} \frac{1 - \alpha}{\alpha} \tag{5}$$

where the quality x is defined as

$$x = \frac{W_v}{W_w + W_v} \tag{6}$$

Homogeneous Model (No Slip)

As previously discussed, the simplest of the flow models is the homogeneous model in which both the liquid and vapor move at the same velocity (no slip). In this case, the homogeneous void fraction is given as

$$\alpha_{HOMO} = \frac{1}{1 + \frac{1 - x}{x} \frac{\rho_v}{\rho_L}} \tag{7}$$

The calculated force for the homogeneous model is found by substituting in equation (2) the values of α computed from equation (7).

Anticipated Error in Force Estimates

From equation (2) it is apparent that the force results will be very sensitive to the void fraction measurements. If the difference between the actual void fraction and the measured void fraction is

$$\alpha - \alpha_{MEAS} = \Delta\alpha$$

then the percentage error in the value of F_{CAL}/F_{MEAS} would be

$$\text{percent error} = \frac{\Delta\alpha}{1 - \alpha} \times 100 \tag{8}$$

From the data shown in figure 3, $\Delta\alpha$ is estimated to be 0.05. Consequently, for values of $\alpha \leq 0.25$ the computed force will have an uncertainty of at least ±6 percent. For $\alpha \leq 0.5$, the uncertainty would increase to at least 10 percent. This uncertainty will be represented by vertical lines in the results, to be presented (figs. 7 and 8).

DISCUSSION OF RESULTS

$\alpha = 0$

For the all liquid case ($\alpha = 0$), a comparison of the calculated to the measured force appears in figure 4 while the ratio of the calculated to measured force as a function of liquid velocity (Reynolds number) is shown in figure 5. As seen in figures 4 and 5, the calculated measured values are within 6 percent of each other. Some of this 6 percent deviation is experimental error and some could be attributed to changes in the velocity profiles over the range of operating conditions. The capacity of the load cell, 22.4 newtons (5 lb_f), limits the maximum flow and thus the upper value of the Reynolds number of 100 000. The lowest Reynolds

number (40 000) is determined by the lower limit to which the pump can be throttled.

Slip Ratio

The slip ratios are shown in figure 6. Data were taken for nominal void fractions of 0.25 and 0.5. The computed slip results are listed in table I. Some of the scatter in the slip ratio results from the measured variations in α. The void fraction varies from 0.45 to 0.55. In addition, it was estimated that the data have an uncertainty of about ±20 percent.

As seen in figure 6, the slip ratio is nominally one when the void fraction is 0.25, but the slip ratio deviates significantly from one at the higher void fraction where $\alpha = 0.5$.

Comparison of Variable Slip (Measured α) and Homogeneous Models

For $\alpha \simeq 0.25$, the ratio of the calculated to the measured force for both the homogeneous and variable slip (measured α) models are in very close agreement with the calibration line, as seen in figure 7. Thus, both of these one-dimensional two phase models appear to be applicable over the entire range of Reynolds numbers tested. This is not surprising since the slip ratios for both models turned out to be near unity. When $\alpha \simeq 0.5$, the slip ratios of the two models differed and they predicted different force values.

The Reynolds number in the abscissa of figure 7 is an all-liquid number. The data shown in figure 7 could just as well have been plotted against liquid velocity.

For $\alpha \simeq 0.5$, significant deviations between the one-dimensional variable slip, no slip (homogeneous), and the measured impulse force are

seen to occur in figure 8. In particular, a steep drop in the one-dimensional variable slip representation is seen in figure 8 near a Reynolds number of 0.4×10^5. For these low Reynolds numbers the variable slip calculation is in error. For larger Reynolds numbers, the variable slip representation seems to be approaching the calibration line, which indicates that this model is accurate at high liquid velocities (Reynolds numbers). This observation is in agreement with reference 5. The drop off in the variable slip model at high Reynolds numbers as suggested in reference 3 was not seen. However, such a trend might occur at higher void fraction.

The homogeneous model fortuitously falls along the unity line in figure 8; which is in close agreement with the results of reference 3. The homogeneous model prediction is approximately 6 percent high, which for practical estimation purposes is quite satisfactory. It should be pointed out, however, that the predicted homogeneous values represent variable α values. The experimental data and the variable slip model are based on a constant α, which was measured by gamma attenuation. The α which one could calculate from the homogeneous expression would not agree generally with the experimentally-determined value.

One-Dimensional Variable Slip (Measured α) Correlation

The drop off in the deviation between the computed variable slip force and the measured force at low Reynolds numbers (~40 000) will now be discussed. Andeen and Griffith (ref. 3) present three possible reasons which might account for the above deviations at low Reynolds numbers: (1) two-dimensional velocity profiles, (2) unsteady fluctuations such as slugging, and (3) turbulent fluctuations. A fourth possi-

ble explanation (4) could be a transition in flow patterns (bubbly, annular, etc.). In an actual situation, a combination of the above mechanism could account for the deviation between prediction and experiment. Each of these reasons will be discussed in detail because any or all of the above reasons can cause the real force to be greater than the one-dimensional variable slip value as calculated in equation (2).

Spatial Velocity Distribution

Two dimensional velocity profiles will lead to higher estimates of the impulse force than would the simple one-dimensional models using an average channel velocity.

For the case where $\alpha = 0$ (all water), if a power law velocity profile assumed for a single phase system is

$$v = v_{MAX}(y/n)^{1/n} \tag{9}$$

then the ratio of the one-dimensional to the two-dimensional force is

$$\frac{F_{1D}}{F_{2D}} = \frac{\left(1 + \frac{2}{n}\right)}{\left(1 + \frac{1}{n}\right)^2} \tag{10}$$

For the Reynolds number range considered herein, a value of $n = 7$ is appropriate (ref. 7). In this case the above ratio is about 0.98. The two-dimensional impulse force is two percent greater than that calculated for the simple one-dimensional case. Physically, since the impulse force is proportional to the velocity squared, the fluid particles with velocities greater than the average will produce a larger contribution to the total force than those below the average.

Could two-dimensional effects produce the high drop off shown in figure 8 for $\alpha = 0.5$? For this to occur, the value of n in the two-

phase fully dispersed flow would of necessity be much smaller than that normally observed in turbulent flow of a single phase fluid. This is not expected. However, for other two-phase flow regimes, such as annular, significant changes in n are possible.

Time Dependent Variations

As mentioned earlier, unsteady fluctuations such as slugging or flow regime transitions will decrease the ratio of the one-dimensional calculated force to the measured force recorded by the load cell. The recorded output of the load cell showed the measured force to be periodic; consequently, time-averaged variations in the velocity must be considered. Figure 9 displays the amplitude of the load cell oscillation, F_{amp}, as a function of the Reynolds number. As seen in figure 9, the force measurement exhibits a significant oscillatory behavior and the amplitude of the oscillations increase with increasing void fraction and decreasing Reynolds number. This is a reflection of a changing flow pattern. At the low void fraction $\alpha = 0.25$, the flow configuration is generally one of bubbles in a continuous liquid stream - bubbly flow. As the void fraction increases, the bubbles coalesce into large gas volumes and the flow pattern might be better characterized as alternate slugs of gas and liquid-slug flow. With this observation, it is interesting to examine analytically what a large scale oscillation will do to the results.

The velocity oscillations which occur near the exit of the tube produce the periodic output of the load cell. Unfortunately, the actual magnitude of the velocity oscillations are unknown. Conceivably, the amplitude of the velocity oscillation could be quite large in comparison

to the mean velocity v.

Since the force exerted by the gas is negligible, we will consider only the liquid phase with cross sectional area A_L in the following calculations. Furthermore, we assume

$$v = \bar{v}(1 + a \cos \omega t) \tag{11}$$

where "a" times $\bar{v}$ represents the amplitude of the oscillation. The flow area A_L will vary with the velocity. A detailed look at the momentum and continuity equation will be required to determine the relationship between v and A_L. For the purpose of simplicity, however, we will assume A_L to be a constant.

To preclude reverse flow, the amplitude factor a is assumed to have a limiting value of 1. During the course of the experiment no visual indications of flow reversal were seen. We will now investigate what effect the amplitude "a" will have on the calculated average force.

The average force for one cycle (period = $2\pi/\omega$) can be calculated as follows.

$$\bar{F}_t = \frac{1}{\left(\frac{2\pi}{\omega}\right)} \int_0^{2\pi/\omega} \frac{\rho A_L v^2}{g_c} dt \tag{12}$$

Substituting equation (11) into equation (12) and integrating gives

$$\bar{F}_t = \frac{\rho A_L v^2}{g_c} \left(1 + \frac{a^2}{2}\right) \tag{13}$$

As seen in the above equation, the average force will be independent of frequency; however, the response of the measuring system will, of course, depend on the frequency. Noting that

$$A_L = A(1 - \alpha) \tag{14}$$

and taking the ratio of equation (2) to equation (13)

$$\frac{\overline{F}_{CAL}}{\overline{F}_t} = \frac{1}{1 + \frac{a^2}{2}} \tag{15}$$

As previously mentioned, for the limiting case of a equal to 1, the lower limit to the ratio given by equation (15) would be

$$\frac{\overline{F}_{CAL}}{\overline{F}_t} = \frac{2}{3} \tag{16}$$

As seen in figure 8, there is an indication that the ratio of the calculated to impulse force approaches the 2/3 value. Some detailed measurements of the velocity leaving the tube would be required to determine if the 2/3 value suggested by equation (16) represents a lower limit to the data or if this is just a fortuitous occurrence. This calculation leaves us with the impression that flow oscillations could drastically affect the momentum results. Unfortunately we cannot draw any strong conclusions regarding this possibility as it applies to the data reported herein.

A word of caution is necessary at this point. Figure 10 displays a ratio of the amplitude of the load cell oscillation, to the mean force amplitude, F, as a function of Reynolds number. As seen in figure 10, the ratio increases significantly at the low Reynolds numbers where the drop off occurred in figure 8. From the results in figure 10, we might expect that the ratio of $\overline{F}_{CAL}/\overline{F}_{MEAS}$ for $\alpha = 0.25$ in figure 7 should display a drop off similar to that shown in figure 8 for $\alpha = 0.5$. This is contrary to the conclusion drawn from figure 9. We suspect, however, that because of damping and frequency response of the momentum cage, the

magnitude of oscillation for the $\alpha = 0.5$ data should be higher. Thus, it may be fortuitous that both sets of data fell on the single curve displayed in figure 10. In our opinion, it is safer to draw conclusion from figure 9 rather than figure 10.

Turbulent Fluctuations

Turbulent fluctuations are somewhat similar to the time dependent fluctuations just discussed, if for example we assume

$$v = \bar{v} + v' \tag{17}$$

where v' is a fluctuation random velocity component. In general, v' could be represented by an infinite Fourier series; however, as rough approximation for turbulent effects, we might assume

$$v = \bar{v}(1 + v'_{MAX} \cos \omega t) \tag{18}$$

where v'_{MAX} is a crude representation of largest intensities seen in the channel. At any position in the channel, v'_{MAX} will generally be less than 0.15. Substituting this value into equation (15) indicates that the turbulent fluctuations may account for less than 1 percent of the drop observed in the calculated to measured force ratio.

Flow Patterns

The experimental flow regime in the test was nominally in the bubbly regime as indicated by the position of the experimental data on the Baker plot shown in figure 10. However, since in reality, the separation of bubbly from slug flow actually occurs over a broad range, a flow transition might be beginning at the lower Reynolds numbers.

CONCLUSIONS

For the range of Reynolds numbers and flow regime investigated, the following conclusion can be made.

1. The one-dimensional variable slip (measured α) and the no-slip homogeneous predictions of the two phase momentum are valid for void fractions equal to or less than 25 percent.

2. For void fractions of about 50 percent, the variable-slip model is valid for large Reynolds numbers. However, for Reynolds numbers below 50 000 a significant deviation between experiment and prediction is seen. The homogeneous no-slip model seems to predict the impulse force for this higher void fraction over the entire Reynolds number range. This observation, which is in agreement with the experimental results in reference 3, is due to the over prediction of the one-dimensional momentum by the homogeneous model in which the slip is assumed to be unity. As illustrated by the data, the homogeneous model is a versatile and useful technique for one-dimensional design calculations in the range of Reynolds numbers investigated.

LIST OF SYMBOLS

A	cross sectional area of duct
A_L	cross sectional flow area of liquid
a	amplitude of velocity fluctuation
$\overline{F}_{CAL}$	average calculated force, equation (2)
F_{1D}	average force for one-dimensional flow (slug)
F_{2D}	average force for two-dimensional flow
$\overline{F}_{MEAS}$	average measured force
$\overline{F}_t$	time averaged force
G_N	nitrogen flow rate, lb m/hr ft^2 for Baker plot
G_w	water flow rate, lb m/hr ft^2 for Baker plot
g_c	gravitational constant

h	1/2-height of channel
P	perimeter
R_w	liquid Reynolds number $4W_w/P\mu_w$
n	turbulent power law coefficient
v	velocity
$\bar{v}$	average velocity
v_{MAX}	maximum velocity
v'	fluctuating turbulent component of v
v'_{MAX}	maximum value of v'
W_N	nitrogen flow rate
W_v	vapor flow rate
W_w	water flow rate
x	quality, equation (6)
y	height coordinate
y^*	y/h
α	void fraction
$\Delta\alpha$	$\alpha - \alpha_{MEAS}$
α_{HOMO}	homogeneous void fraction
α_{MEAS}	measured void fraction
λ	equals $[(\rho_N/0.075)/\rho_w/62.3]^{1/2}$ (for Baker plot)
μ	viscosity of water, centipoise for Baker plot
ρ	density
ρ_L	liquid density
ρ_n	density of nitrogen, lb m/ft^3 for Baker plot
ρ_v	vapor density
ρ_w	density of water, lb m/ft^3 for Baker plot

ϕ gamma signal

ϕ_f gamma signal for all water

ϕ_o empty gamma signal for all nitrogen

ψ equals $(73/\sigma)\left[\mu_L(62.3/\rho_L)^2\right]^{-1/3}$ (For Baker plot)

ω angular velocity

REFERENCES

1. Martinelli, R. C., and D. B. Nelson, Trans. ASME, 70, 695 (1948).

2. Lockhart, R. W., and R. C. Martinelli, Chem. Eng. Prog., 45, 39 (1949).

3. Andeen, G. B., and P. Griffith, J. Heat Transfer, 90, 211 (1968).

4. Henry, R. E., Argonne National Lab. Report ANL-7430 (1968).

5. Henry R. E., and H. K. Fauske, J. Heat Transfer, 90, 220 (1968).

6. Hooker, H. H., and G. F. Popper, Argonne National Lab. Report ANL-5766 (1958).

7. Schlichting, H., "Boundary Layer Theory," p. 505, 4th ed., McGraw-Hill, New York (1960).

TABLE I. - DATA

RUN	W_N (lb/sec)	W_W (lb/sec)	R_W	F_{MEAS} (lb)	Quality	α_{MEAS}
1-710323	0.	0.184E+01	0.705E+05	2.20	0.	0.
2-710323	0.	0.840E+00	0.379E+05	0.48	0.	0.
3-710323	0.	0.844E+00	0.414E+05	0.47	0	0.
4-710323	0.147E-02	0.844E+00	0.424E+05	1.00	0.174E-02	0.526
5-710323	0.	0.774E+00	0.398E+05	0.41	0.	0.
6-710323	0.	0.774E+00	0.399E+05	0.42	0.	0.
7-710323	0.143E-02	0.777E+00	0.401E+05	1.01	0.183E-02	0.480
1-710330	0.	0.176E+01	0.637E+05	2.09	0.	0.
2-710330	0.209E-02	0.142E+01	0.651E+05	3.54	0.128E-02	0.460
3-710330	0.	0.125E+01	0.548E+05	1.06	0.	0.
4-710330	0.173E-02	0.123E+01	0.545E+05	2.05	0.141E-02	0.524
5-710330	0.	0.108E+01	0.502E+05	0.79	0.	0.
6-710330	0.169E-02	0.114E+01	0.547E+05	1.65	0.148E-02	0.430
7-710330	0.174E-02	0.124E+01	0.586E+05	2.05	0.140E-02	0.430
8-710330	0.	0.846E+00	0.422E+05	0.49	0.	0.
9-710330	0.144E-02	0.851E+00	0.434E+05	1.11	0.169E-02	0.438
10-710330	0.	0.774E+00	0.399E+05	0.41	0.	0.
11-710330	0.142E-02	0.777E+00	0.401E+05	0.99	0.183E-02	0.505
1-710413	0.	0.182E+01	0.655E+05	2.09	0.	0.
2-710413	0.637E-03	0.176E+01	0.695E+05	2.74	0.361E-03	0.176
3-710413	0.	0.126E+01	0.538E+05	1.05	0.	0.
4-710413	0.455E-03	0.126E+01	0.563E+05	1.40	0.361E-03	0.209
5-710413	0.	0.110E+01	0.509E+05	0.81	0.	0.
6-710413	0.388E-03	0.110E+01	0.521E+05	1.05	0.353E-03	0.243
7-710413	0.	0.856E+00	0.432E+05	0.49	0.	0.
8-710413	0.322E-03	0.856E+00	0.435E+05	0.65	0.376E-03	0.262
9-710413	0.	0.776E+00	0.400E+05	0.40	0.	0.
10-710413	0.292E-03	0.781E+00	0.402E+05	0.54	0.373E-03	0.246
1-710427	0.	0.183E+01	0.693E+05	2.26	0.	0.
2-710427	0.633E-03	0.178E+01	0.720E+05	2.82	0.355E-03	0.272
3-710427	0.	0.127E+01	0.548E+05	1.11	0.	0.
4-710427	0.458E-03	0.127E+01	0.563E+05	1.45	0.359E-03	0.273
5-710427	0.	0.111E+01	0.502E+05	0.84	0.	0.
6-710427	0.382E-03	0.111E+01	0.519E+05	1.06	0.344E-03	0.247
7-710427	0.	0.861E+00	0.430E+05	0.49	0.	0.
8-710427	0.326E-03	0.856E+00	0.427E+05	0.65	0.380E-03	0.271
9-710427	0.	0.784E+00	0.391E+05	0.40	0.	0.
10-710427	0.282E-03	0.783E+00	0.406E+05	0.54	0.373E-03	0.253
11-710427	0.	0.850E+00	0.440E+05	0.48	0.	0.
12-710427	0.144E-02	0.851E+00	0.436E+05	1.15	0.169E-02	0.463
13-710427	0.	0.793E+00	0.405E+05	0.41	0.	0.
14-710427	0.143E-02	0.783E+00	0.405E+05	1.03	0.183E-02	0.432
1-710506	0.	0.178E+01	0.661E+05	2.12	0.	0.
2-710506	0.215E-02	0.162E+01	0.674E+05	3.66	0.132E-02	0.472
3-710506	0.	0.204E+01	0.862E+05	2.78	0.	0.
4-710506	0.226E-02	0.196E+01	0.825E+05	4.55	0.122E-02	0.472
5-710506	0.	0.220E+01	0.970E+05	3.21	0.	0.
6-710506	0.252E-02	0.195E+01	0.877E+05	5.18	0.134E-02	0.476
7-710506	0.	0.233E+01	0.106E+06	3.75	0.	0.
8-710506	0.207E-02	0.207E+01	0.931E+05	5.94	0.148E-02	0.434
1-710525	0.	0.193E+01	0.719E+05	2.25	0.	0.
2-710525	0.638E-03	0.180E+01	0.773E+05	2.80	0.355E-03	0.201
3-710525	0.220E-02	0.170E+01	0.798E+05	3.95	0.129E-02	0.485
1-710603	0.	0.184E+01	0.730E+05	2.23	0.	0.
2-710603	0.287E-02	0.165E+01	0.724E+05	4.13	0.174E-02	0.542
3-710603	0.	0.204E+01	0.888E+05	2.77	0.	0.
4-710603	0.304E-02	0.181E+01	0.813E+05	4.86	0.168E-02	0.535
5-710603	0.	0.220E+01	0.977E+05	3.20	0.	0.
6-710603	0.286E-02	0.184E+01	0.882E+05	5.24	0.153E-02	0.535
7-710603	0.	0.204E+01	0.927E+05	2.80	0.	0.
8-710603	0.301E-02	0.182E+01	0.830E+05	4.86	0.165E-02	0.535
9-710603	0.	0.783E+00	0.400E+05	0.40	0.	0.
10-710603	0.145E-02	0.789E+00	0.401E+05	1.02	0.184E-02	0.542

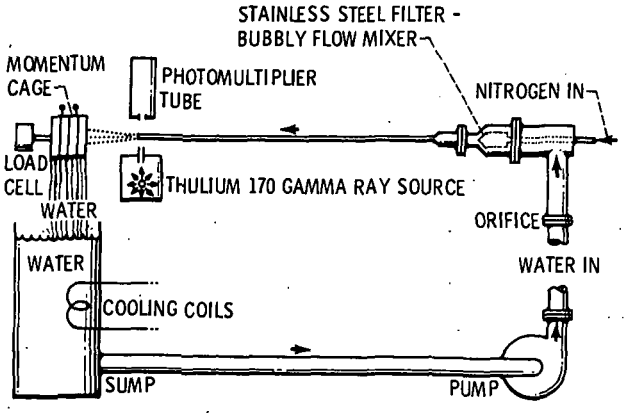

Figure 1. - Momentum pressure drop apparatus.

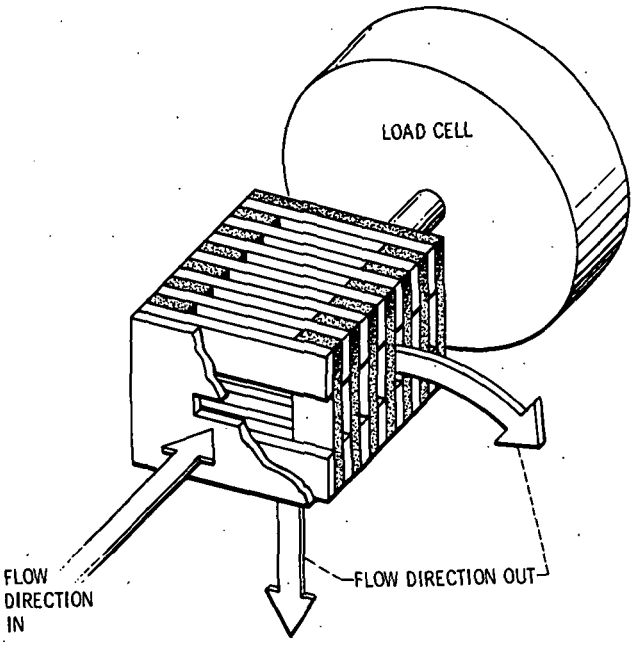

Figure 2. - Momentum cage and load cell.

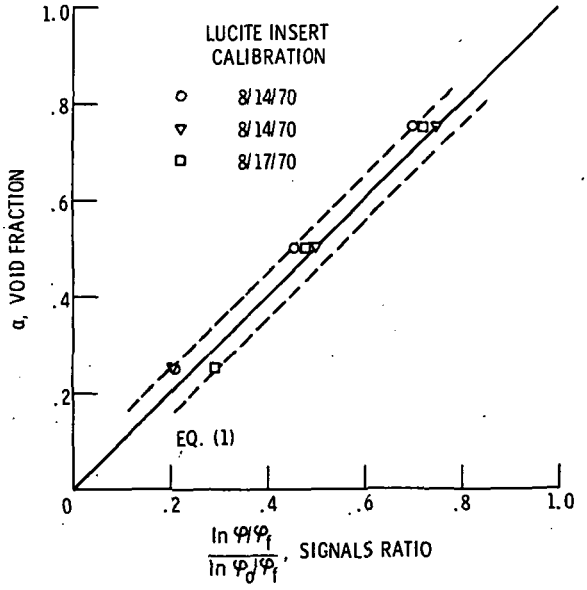

Figure 3. - Comparison of theoretical and calibrated void as determined from gamma-ray attenuation experiment.

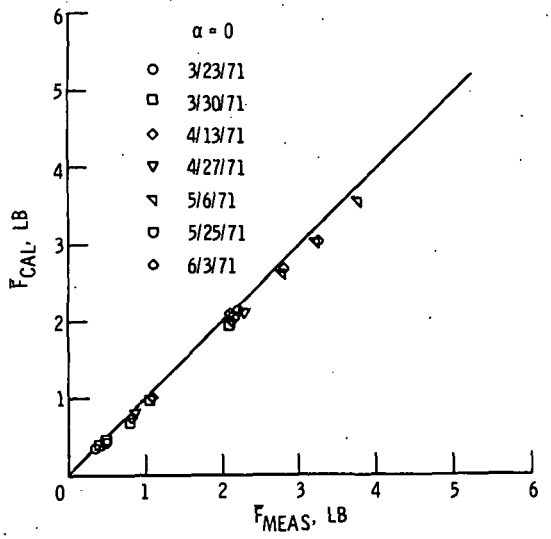

Figure 4. - Comparison of measured to calculated force for zero void fraction - all liquid.

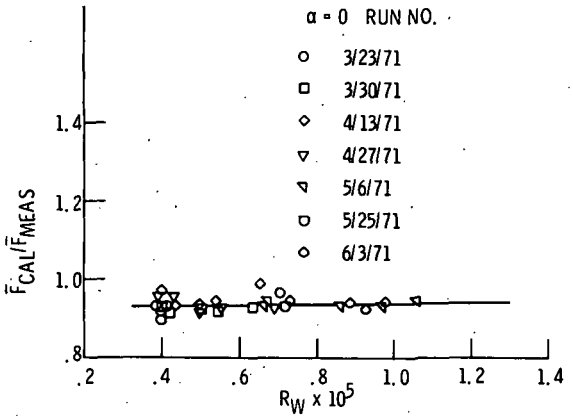

Figure 5. - Ratio of force calculated from one dimensional assumption to measured force for $\alpha = 0$.

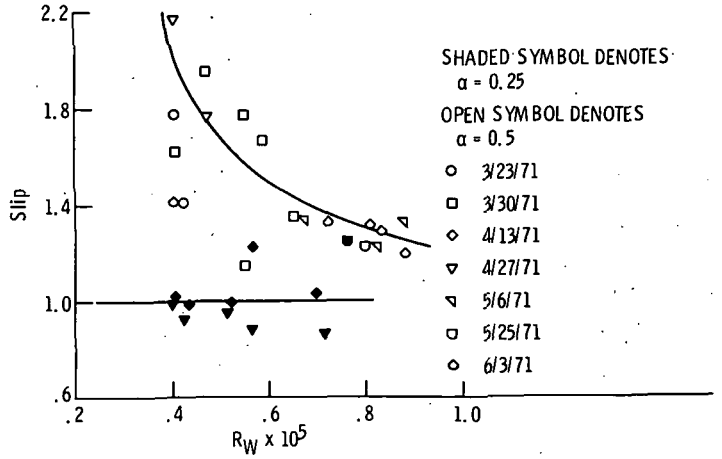

Figure 6. - Measured slip ratios.

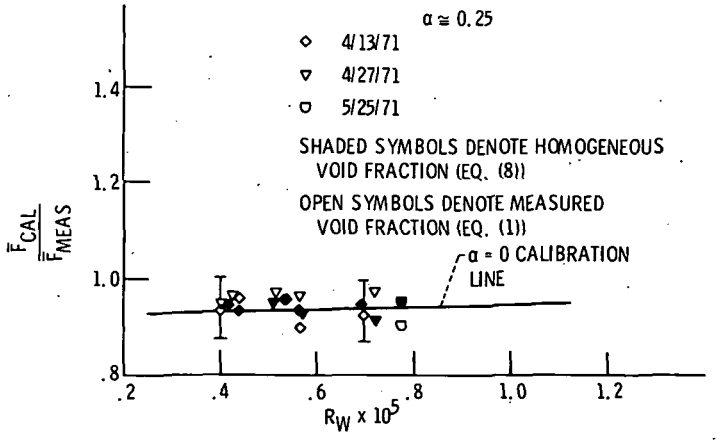

Figure 7. - Ratio of force calculated from one dimensional assumption to measure force for $\alpha = 0.25$.

E-6871

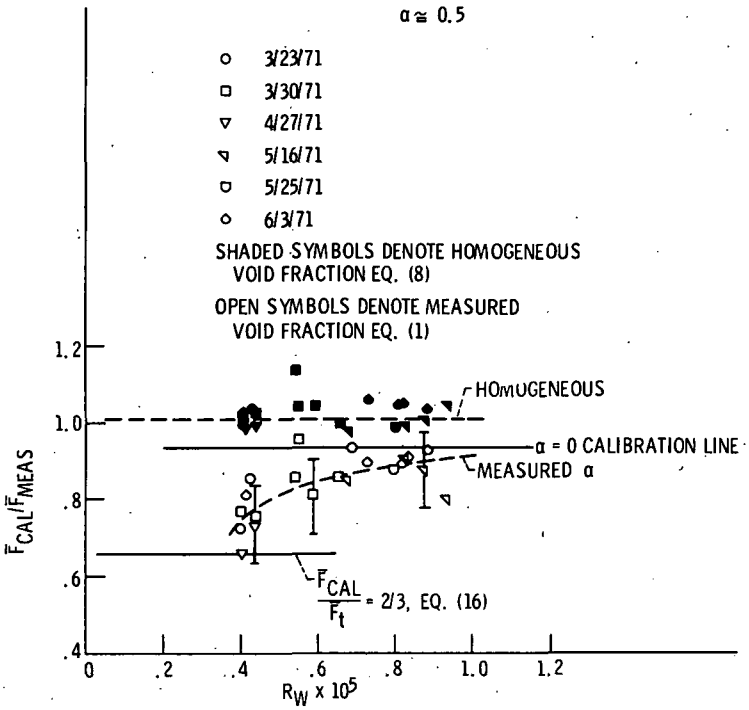

Figure 8. - Ratio of force calculated from one dimensional assumptions to measured force for α = 0.5.

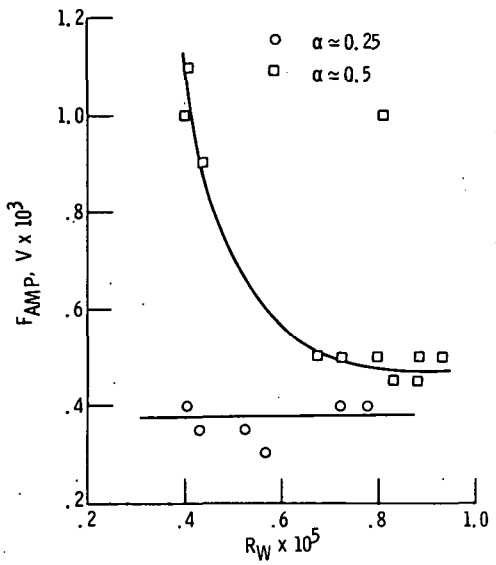

Figure 9. - Amplitude of measured force for α ≃ 0.25 and 0.5.

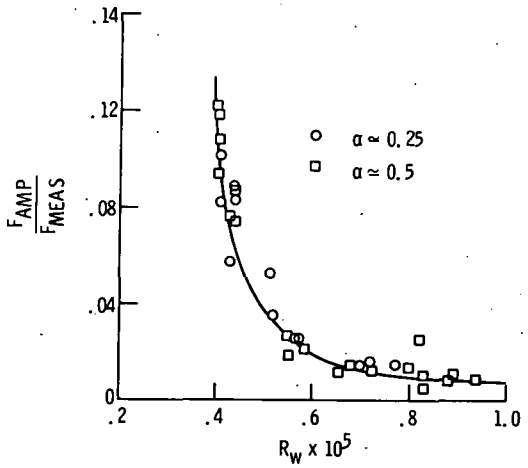

Figure 10. - Ratio of amplitude to measured force.

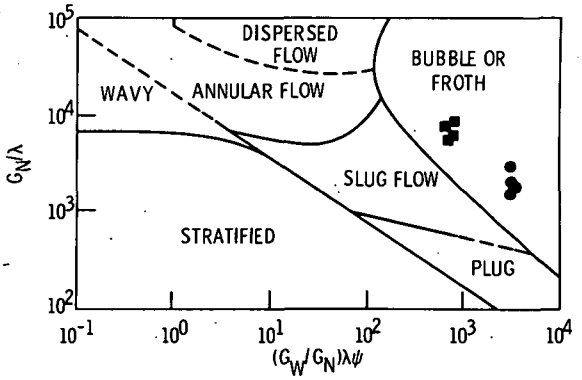

Figure 11. - Flow regimes of data as designed by baker plot.